

**Multi-model Estimates of Atmospheric Response to Modes of SST Variability and
Implications for Droughts**

Philip J. Pegion* and Arun Kumar

Climate Prediction Center, NOAA/NWS/NCEP, Camp Springs, MD

*current affiliation: CIRES, Boulder Colorado

**To be Submitted to the Journal of Climate for consideration in the
USCLIVAR Drought Working Group Special Issue**

Abstract

A set of idealized global model experiments was performed as part of the U.S. CLIVAR Drought Working Group by several modeling centers. The purpose of the experiments was to assess the role of the leading modes of sea surface temperature (SST) variability on the climate over the continents, with particular emphasis on the influence of SSTs on surface climate variability and droughts over the U.S. An analysis based on several models gives more creditability to the results since it relies on the assessment of impacts that are robust across different models.

Coordinated atmospheric general circulation model (AGCM) simulations forced with three modes of SST variability were analyzed. The results show that the SST forced precipitation variability over the central United States is dominated by the SST mode with maximum loading in the central Pacific Ocean. The SST mode with loading in the Atlantic Ocean, and a mode that is dominated by trend in SSTs, lead to a smaller response.

Based on the response to the idealized SSTs, the precipitation response for the 20th century was also reconstructed. A comparison with the AMIP simulations forced with the observed SSTs illustrates that reconstructed precipitation variability was similar to the one in the AMIP simulations, further supporting the conclusion that the SST modes identified in the present analysis play a dominant role in the precipitation variability over the U.S. One notable exception is the Dust Bowl of the 1930s, and further analysis regarding this major climate extreme is discussed.

1. Introduction

Towards identifying the causal mechanism for the occurrences of long-term droughts, the U.S. CLIVAR Drought Working Group (DWG) was formed in December 2006. The approach of the DWG was to coordinate evaluations of existing model simulations, and to also coordinate new experiments designed to address some of the outstanding questions related to drought variability and predictability. Six modeling groups joined in the effort and produced a wealth of model simulation. The primary goal of the focused effort was to quantify the role sea surface temperature (SST) variability on changes in the atmospheric circulation and terrestrial climate.

Various large scale patterns of sea surface temperature (SST) variability have been known for many years. A dominant mode of SST variability is associated with the El Niño – Southern Oscillation (ENSO). Other well known modes of SST variability include Pacific Decadal Oscillation (PDO) for the northern Pacific (Mantua et al. 1997), Interdecadal Pacific Oscillation (IPO) the basin wide pattern (Power et. 1999) north Atlantic multi-decadal oscillation (AMO) (Enfield et al. 2001), Indian Ocean Dipole (IOD) (Saji et al. 1999). In addition to the quasi-periodic modes of SST variability, trends in the SSTs, for example, an upward trend in SSTs in all tropical ocean basins, have also been identified.

Modes of SST variability have also been linked to the atmospheric and terrestrial climate variability over different regions of the globe. For example, changes in north pacific SST have been associated with droughts in the western and central United States (Namais 1969, 1983). Long term precipitation variability over the U.S. Great Plains has been linked to SST anomalies across a wide swath of the Pacific ocean (Schubert et al. 2004). Hoerling and Kumar (2003) identified the importance of SST anomalies outside of the tropical Pacific, and demonstrated the

role SSTs in the Indian Ocean have on the hydro-climate of the United States that also extends across a latitudinal belt in the Northern Hemisphere. More recently the persistent La Nina of the late 20th early 21st century has been linked to the multi-year drought of the western United States. (Seager et al. 2005)

Leveraging on the set of coordinated atmospheric general circulation model (AGCM) simulations that were part of the DWG, the present analysis looks at the relationship between the leading patterns of SST variability and their influence on the climate over land areas. The analysis includes (1) observed relationship of the trend, Pacific, and Atlantic mode of SST variability with precipitation and surface air temperature, (2) influence of the modes of SST variability on the atmospheric and terrestrial climate in idealized AGCM simulations, and (3) to what extent the variability in the AGCM simulations forced with observed SSTs (in the so called AMIP simulations) can be reproduced based on the response inferred from the idealized AGCM simulations.

The identification of the leading patterns of SST variability is described in section 2. A description of the observed data and models used in the study is in section 3. The AGCM simulations are described in section 4. The results are presented in section 5, and section 6 contains the conclusions.

2. Identification of the leading modes of SST variability

The leading patterns of sea surface temperature (SST) variability are identified based on a rotated empirical orthogonal function (REOF) analysis of annual mean HADISSTv1 SSTs (Rayner et al. 2003). The fifteen leading EOFs were rotated using varimax rotation (Kaiser

1958). In order to avoid contamination of sea-ice points, the analysis was restricted to grid points that were completely ice free for the years 1901-2004. The leading mode of variability in this analysis is the trend of global SSTs, which explains 27.2% of the annual mean SST variance. Then second leading mode is an ENSO like pattern and explains 20.5% of the variance. The third mode, which represents only 5.8% of the global variance, is a north Atlantic Pattern, and is similar to the Atlantic multi-decadal oscillation.

The spatial pattern of the leading REOF shows a fairly uniform loading throughout the world's oceans (Fig. 1). The highest loading occurs in the southern Indian Ocean, and there is a noticeable minimum in the central tropical Pacific Ocean. The principle component associated with this leading pattern shows a non secular increase, with the values remaining nearly constant from 1901 to about 1930, then increase sharply from 1930 to 1944. Then for about 30 years, the values remain near zero. From the mid 1960s to the mid 1980 the amplitude of the time-series increases more rapidly with a gradual increase after that.

The second REOF is dominated the variability in the central Pacific associated with the ENSO. Warm SSTs in the tropical central and eastern pacific are flanked by SST anomalies of the opposite sign to the northwest and southwest. There are also weak positive anomalies in the Indian and Atlantic oceans that are generally associated with remote oceanic response to the SST variability in the Pacific (Alexander et. al 2002). The associated time series is dominated by variability on the inter-annual time-scale, but there is evidence of variability on a slower time-scale associated with waxing and waning of ENSO in different decades (Xue et al. 2003; Tang et al. 2008), and also with preponderance of ENSO with a particular phase, for example, with the periods of 1950 to 1970 dominated by the La Niña events.

The third REOF has most of its loading in the North Atlantic Ocean and explains 28.9% of variability in the tropical North Atlantic basin alone. The spatial pattern resembles the North Atlantic Multi-decadal oscillation (AMO, Enfield et al. 2001). The time series has large swings and a distinct low frequency behavior. The period from 1901 to about 1930 is predominately associated with negative phase, followed by 1930s to 1970 of dominantly positive phase. The phase of pattern shifts back to a negative phase from 1970-1994, before reverting to a positive phase after 1995.

3. Data and Models

The six modeling groups that participated in coordinated model simulations as part of the DWG were NASA-GSFC, LDEO, GFDL, UMD/NCAR, UM/COLA, NCEP/CPC. Five of the groups, with the exception of UM/COLA preformed the experiments with a global AGCM forced with the identical SSTs. UM/COLA did the experiments with a coupled model. The atmospheric models participating in the experiments were the NSIPP1 AGCM (Bacmeister et al. 2000; Schubert et al. 2004), CCM3 (Kiehl et al. 1998; Seager et al. 2005), GFDL AM2.1 (Delwoth et al. 2006; The GFDL Model Development Team 2004, Milly and Shmakin 2002), CAM3.5, and the NCEP GFS (Campana and Caplan 2005). These five models have diverse developmental histories, and comprise of both spectral and grid-point models, different physical parameterizations and spatial resolutions. More details about the individual models can be obtains in the references included above or in Schubert et al. (2009).

Beside the HADISSTv1 SST data, other observational datasets include: gridded observed precipitation from the global historical climate network GHCN on a 5x5 degree grid (Vose et al.

1992); surface temperature observations from the Hadley center's HadCRUT3 (Brohan et al. 2006), that incorporates both land and sea surface temperature observations on a 5x5 degree grid.

4. AGCM Experiments

The five modeling groups executed a series of idealized AGCM simulations, and four of them also provided long simulations forced with observed SSTs over the 20th Century. Every group did not include all of the experiments, nor did every group produce an ensemble of AMIP type long simulations to quantify climate variability over the entire 20th century. Specific AGCM simulations are next described.

a. AGCM simulations with idealized SSTs

The purpose of the idealized experiments was to isolate the atmospheric and terrestrial influence of each SST pattern separately as it is difficult to do so either in the AMIP simulations or in the observations. To assess the relative role of each SST pattern, a series of AGCM simulations forced with the spatial pattern of SST associated with the first three REOFs were completed.

The sets of experiments consisted of each modeling group running their respective AGCM with a repeating seasonal cycle of climatological SSTs, and also with fixed anomalies added to the repeating seasonal cycle. The patterns were scaled by +/- the standard deviation of the principal component. The trend was scaled by one standard deviation, which roughly represents a period of 1901-1942 for the negative scaling, and 1965-2004 for the positive period. The Pacific and the Atlantic REOFs were scaled by twice the standard deviation to emphasize

their atmospheric influence. The anomaly patterns were then added to a repeating climatological seasonal cycle based on HADISST data, with the climatology based on the 1901-1999 period. The treatment of sea-ice climatology was left to the individual modeling groups. To isolate the role of each of the SST pattern, the anomalies for the Pacific pattern were set to zero in the Atlantic Basin, and conversely, the anomalies in the Pacific and Indian oceans were set to zero for the North Atlantic forcing pattern.

Each modeling center ran several long simulations with the idealized SST patterns, and a control run with the climatological SSTs. The runs varied between 36 years (NCEP GFS) to 51 years for the other models with the first year discarded as spin-up. Both the positive and negative polarity of each pattern was used to force the AGCM simulations. In addition, various combinations of patterns were also used in additional experiments. In total, there were 15 different experiments run with specified SST patterns. The results presented in this paper are for the model response to each of the individual SST patterns, and does not address how the atmospheric response to the SST patterns interplay with each other, or the relative role of the tropical vs. extra-tropical SSTs.

b) AMIP Simulations

Several of the modeling groups also ran an ensemble of long AMIP simulations forced with observed SST: NSIPP 14 members, GFDL 10 members, CCM3 16 members, and CAM3.5 1 member. The ensemble of simulations were generated by perturbing the atmospheric initial conditions at the initial time of the integration and allowing the model atmospheric and land state to evolve freely over the observed monthly SST data.

A multi-model mean (MMM) from all of the AMIP simulations was created for the analysis. MMM was produced by removing (1) the model's respective climatology for the years 1902-1999 (common years among all the AMIP simulations used), and (2) averaging all 41 members together to create a multi-model ensemble mean. Averaging across such a large ensemble, and across 4 AGCM, greatly minimizes the internal noise in the atmospheric variability. Further, averaging across the four models also decreases the impact of model biases, although the procedure is not perfect since the size of the ensemble is not uniform across models.

5. Results

a) Observed relationship

We first analyze at the observed temperature and precipitation to see if there is a relationship between these meteorological variables and three modes of SSTs. Composites based on +/- one standard deviation of the three leading principal components were created to quantify the observed relationship (Fig. 2).

For the composites associated with the trend mode (Fig. 2, top panels), it is apparent that there is a positive precipitation trend over the eastern part of the United States and Australia. In addition, most of the land areas with data coverage show an increase in temperature. An exception is a tendency towards cooler temperatures in the southeast United States. The trends over the U.S. are similar to ones reported by Robinson et al. (2002), Kunkel et al. (2006), Wang et al. (2009) among others.

The composites of the Pacific SST pattern (Fig. 2, middle panels) show an increase in

precipitation over the central and southern United States, and a decreased precipitation covering most of Australia. The temperature composite shows warming over the northern and western portions of the U.S., and cooler temperatures over the southern tier states. There are also below average temperatures covering eastern Europe.

The composites of the Atlantic pattern (Fig. 2, bottom panels) show signs of decreased precipitation over parts of the US, Hawaii, northern Australia, and an increase over Europe. The temperature composite shows warmer than average temperatures for most of the North America.

b) Relationship in AGCM Simulations

The observed temperature and precipitation composites are next compared with the composites based on the multi-model mean of AMIP simulations. Composites based on the principle components of the three leading SST REOFs are computed in the same way as for the observations. Since the AGCM do not have the spatial sampling problems that observations have, the AGCM based composites provide a coherent spatial structure of how the atmosphere *responds* to various SST patterns. Further, as the AMIP composites are based on averaging over 41 member ensemble, a process that minimizes the influence of the atmospheric internal variability, the statistical significance of the composite is also high.

The composites based on the AMIP simulations are shown in Fig. 3. The precipitation response to the SST trend pattern (Fig. 3, top panels) is mostly limited to the tropical oceans, but the temperature composites show broad areas of warmer temperatures. In contrast to a same sign trend in SSTs except in the eastern Pacific, the precipitation response has both positive and negative rainfall anomalies. This is consistent with mass continuity across pressure surface such

that increased precipitation, and associated increase in vertical motion, has to be balanced by increased downward motion, and decreased precipitation (Kumar et al. 2004; Chou et al. 2006). On the other hand, temperature and 200-mb response show a positive anomaly almost everywhere, and is similar to documented influence of warmer SSTs (Hoerling et al. 2008; Compo and Sardeshmukh 2008).

The response to the Pacific SSTs (Fig. 3, middle panel) is similar to the observations, with increase in precipitation over Central North America, South America, and decrease over the Maritime continent and Australia. Since the models are globally complete, response over the open ocean can also be inferred. Increased precipitation is found near the date line and is surrounded by a horseshoe pattern of negative precipitation anomalies. The temperature response is also similar to observations with warm temperatures over the Western Canada, cooler temperatures over the southern U.S. and a warming over tropical land areas, and is similar to known ENSO impact (Peng et al. 2000).

The precipitation response to the changes of tropical Atlantic SSTs (Fig. 3, bottom panels) show an increase where the SSTs are also positive, and a decrease over the Gulf of Mexico extending northward into the contiguous United States. There is also a decrease of precipitation that extends across nearly the entire Pacific Basin. The temperature response to this SST forcing causes warmer than average temperature for central North America and for much of Eurasia.

c) Atmospheric Response in the AGCM simulations with Idealized SSTs

A potential caveat with the composite analysis based on the observed data and the AMIP

simulations is that the SST modes never occur in isolation, and hence, the corresponding atmospheric response could have contributions from other SST anomalies. This shortcoming is rectified based on the analysis of AMIP simulations forced with idealized AGCM simulation where SST forcing for one mode at a time is specified.

The atmospheric response in the idealized experiments is defined as the multi-model mean of the positive polarity minus the negative polarity experiments for each SST mode. The annual mean response in temperature, precipitation and 200 mb height for the three leading SST patterns is shown in Fig. 4. Apart from the composite based on the multi-model mean, agreement between model responses for different SST forcing patterns is also assessed. To quantify the agreement in the *sign of the ensemble mean response*, regions shaded in Fig. 4 are where at least four out of the five models agree (three out of four for the trend as CCM3.5 did not complete AGCM simulations with the negative trend in SSTs) on the sign of the response.

The precipitation response to the trend SST pattern is mainly confined over the ocean, and coastal regions. The response includes an increase in precipitation over the southern tip of India, extending eastward through the maritime continent, with a decrease of precipitation over the central equatorial pacific. There is also an increase in precipitation over Central America. The temperature response is for a warming over most of the globe. We also note that the spatial pattern of the response to the trend SST pattern in the idealized simulations matches quite well with the composite response inferred based on the AMIP simulations. The 200 mb height response to the trend shows a large scale increase in heights in the tropics and mid-latitudes. The increase in heights is maximized just south of the Aleutian islands and southern parts of the Pacific Ocean.

The Pacific SST pattern (Fig. 4, middle panels) has a more robust response, with increased precipitation over most of the equatorial Pacific, a decrease over the maritime continent. There is also a decrease in precipitation over the Amazon and extending across the tropical Atlantic Ocean into Africa, and an increase in precipitation over North America and the southern portion of South America. The temperature response shows warming over the tropical landmasses and over northwestern Canada into Alaska, and a cooling over the central United States. The height response shows symmetry across both the northern and southern hemispheres with the largest height departures east of the Dateline and just off of the equator and negative height pole-ward and west of the maximum positive response. In general, the spatial pattern for the precipitation and temperature composites matches remarkably well with the one inferred from the AMIP simulations with the observed evolution of SSTs.

The precipitation response to the North Atlantic SST pattern shows an increase over the regions of positive SST anomalies, and reduced precipitation for most of the globe, with the exception over the Indonesian region. The surface temperature response is a large scale warming that extends across northern Africa and into southern Asia. There is also a signal of increased surface temperature response over the southern Great Plains, and Mexico, and central South America. The height response shows an increase in heights over the tropical Atlantic sector and a decrease in heights in the higher latitudes of both hemispheres, but having a larger zonal extent in the southern hemisphere.

d) Analysis of Change in the Probability Distribution Function of Precipitation

It is a well known fact that for a given SST forcing, the time-averaged atmospheric state

is not unique, and has to be characterized by a probability density function (PDF) (Kumar and Hoerling 2000). The analysis of the composites only provides inference about the mean atmospheric response to changes in SSTs. It is feasible that even though the influence of SSTs on the mean of the PDF may be small (as is the case for the precipitation response for the trend and the Atlantic SST pattern), changes in the extremes of the PDF may still be appreciable. To assess this possibility, the PDF of *annual mean* precipitation anomalies for the Great Plains for three SST modes is analyzed (Fig. 5). The Great Plains region is chosen because of observational evidence for the long-term droughts (Seager et al. 2005). The PDF of annual mean precipitation are constructed for the positive and negative phases of SST anomalies separately.

The greatest separation in the PDF of the annual mean precipitation over the Great Plains is for the Pacific SST mode, followed by weaker influence for the Atlantic SST mode. The influence of the trend SST mode is small and also does not indicate an evidence for changes in the extremes for the annual mean precipitation.

One goal of the DWG was to understand the relationship between the long-term droughts and SST variability in different ocean basins. Assuming that precipitation deficits are also related to drought indices, we quantify odds for below normal precipitation anomalies for several years in a row. For this purpose, simulations from all of the models are pooled together, and annual mean precipitation are re-sampled to calculate the odds of having below normal precipitation anomalies three years in a row. The samples of annual mean of precipitation are drawn with replacement, and odds are calculated by counting how many times the sample contained all three years of negative precipitation anomalies. The re-sampling was done 1,000,000 times for each SST pattern. If the annual mean precipitation is a random variable

with a normal distributed, the expected probability for 3-years in a row of below normal precipitation is 12.5%. A drawn sample having all 3 years contain a negative precipitation anomaly is counted as a falling into the 3 dry-years category, if any of the 3 years had a positive anomaly, then it doesn't count as a having 3 dry-years in this estimate.

The Monte Carlo estimate for the warm Pacific SST pattern shows only a 0.1 % chance of having 3 years in a row of below average precipitation, compared to 78.9% when the Pacific is cool. The Atlantic SST pattern forces a shift in probability from 36.5% chance of having 3 dry years in the warm phase versus a 3.5% chance when it is cool. The Trend SST pattern shifts the chance to 24.0% for the warm pattern compared to 6.7% when the SSTs were cool. The climatology runs for all of the models pooled together give a chance of 13.0 percent chance of having 3 dry years. The deviation from 12.5% is due to the skewness of precipitation. The complete results, including analysis for precipitation averaged over other geographical regions, are shown in Table 2. These estimates show that long-term multiyear rainfall deficits (and long-term droughts) are most likely to occur when the Pacific Ocean is Cool or the Atlantic Ocean is warm. The analysis also shows that the likelihood of having a long-term drought increased in response to the linear trend SST pattern. We should point out that precipitation deficit as a proxy for droughts does not include influence of increase in temperatures, and which by increasing evapotranspiration can also lead to hydrological stress and could be a major contributor to water balance (Easterling et al. 2007)

e) Re-construction of precipitation variability in AMIP simulation

In the final analysis, the inferred atmospheric and terrestrial responses related to the three modes of SSTs are used to reconstruct the climate variability for the 20th century. Recall that to

increase the signal-to-noise and to make the identification of the atmospheric response easier, for the idealized experiments the amplitudes of the modes of SST variability were multiplied by a constant factor. Assuming that the response to each SST pattern is linear, the reconstruction is based on the summing up the idealized responses for annual means to the three SST modes (with the response to each pattern scaled by the normalized PC value for that year). The reconstructed response for 1900-2004 is compared with the SST response in the AMIP simulations to assess the role of three discrete modes of SSTs.

The temporal coherence between the reconstructed and AMIP simulated response for precipitation, surface temperature, and 200-mb heights is assessed based on the anomaly correlation. The spatial pattern of temporal correlation for each grid point is shown in Fig. 6. Over the oceans, the correlations for temperature are highest where the loading patterns of the REOFs are also highest. The correlation is also high over most of the continental land masses, particularly in the tropical latitudes. The precipitation correlations are smaller away from the direct influence of the SST variability. Two regions of largest correlation over continental regions are the central United States, and an area extending eastward from the Black Sea in Europe. Finally, most of the SST forced variability for the AMIP simulated 200-mb Heights is associated with the three leading SST modes. We should point out that this analysis is for reconstructing the SST ensemble mean response based on the sum of response due to the leading modes of SSTs, and does not include contribution from atmospheric internal variability.

To focus on the precipitation variability over the Great Plains region alone, time series of annual precipitation from the AMIP simulations and the reconstruction based on the idealized experiments is shown in Fig. 7. The correlation between the two time series is 0.9. Analysis of

contribution from each mode indicates that the largest contribution is because of the Pacific SST mode (not shown). One of the largest differences between the two time-series occurs during the Dust Bowl period of the 1930s. While the AMIP runs show dry conditions during this time, the analysis based on the reconstruction, on average, shows weaker negative anomalies.

The reconstruction approach can also be used to assess the influence of different SST analyses on the inferred precipitation response over the US. To the extent the atmospheric response based on the idealized AGCM simulations is additive, and can be scaled according to the amplitude of the respective SST modes (as is evident from the high correlation between the two time-series in Fig. 7), this is a viable approach without redoing the AMIP simulations with an alternate SST analyses.

One alternate SST analysis we consider is the ERSSTv3b, which is similar to ERSSTv3, but withholds all of the satellite data to provide a more uniform SST record (Smith et al. 2008, Xue et al. 2003). Fig. 8 compares the projection of the ERSSTv3b and HADISST SSTs on to the three leading REOFs for the Dust Bowl period to illustrate the uncertainty in the SST estimate for the 1930s. The SST composite for 1932-1938 from the HADISST (Fig 8a) data shows a weak cool anomaly extending from the central equatorial Pacific ocean east and north to the California coast and the North Pacific ocean is also cool between 30 and 40 degrees North. In contrast, the ERSSv3b (Fig 8c) data shows a substantial cool SST anomaly near the Dateline and equator with the largest negative anomaly of less than -0.6 C, and the SSTs across the North Pacific Ocean the SST anomalies are warmer than the HADISST. The projection of the SST data onto the first three rotated EOFs is shown on the right hand side of the figure. The HADISST data produces a weak projection on these three EOFs (Fig 8b), with the trend pattern

dominating (refer to Figure 1). The projection of the ERSST data shows a much stronger projection onto the Pacific Pattern and also a warmer Atlantic Ocean (Fig 8d).

As the projection of two SST datasets on the three leading REOFs is appreciably different, we also assess the influence of differences in SSTs for the climate over the US based on the reconstruction. Compared in Fig. 9 are the surface temperature and precipitation anomalies averaged over the Dust Bowl period. As indicated in the time series in Fig. 7, the reconstructed precipitation anomalies based on the HADISST are weaker than the corresponding AMIP simulations, Consistent with the weaker precipitation, surface reconstructed temperature anomalies are also weaker than for the AMIP. Further, both surface temperature and precipitation anomalies are also weaker than for the observations, and are shifted southeastward. Because of the stronger amplitude of the projection of the ERSSTvb3 on the three leading SST REOFs, the reconstructed surface temperature and precipitation response over the US is stronger. Since the spatial structure of the reconstructed anomalies is constrained to be invariant, the differences are highlighted by difference in amplitudes of the reconstructed anomalies. This simple analysis highlights the importance of differences in the SST analysis on the understanding, and attribution, of climate variability in the 20th century, particularly for the earlier period when large errors in the SST analysis due to data scarcity exist.

6. Conclusion

In this paper, the influence of the leading modes of SST variability on the terrestrial climate, with a particular focus over the US, was studied. The analysis approach included identification of the leading modes of SST variability, and a coordinated set of AGCM simulations forced with the SST modes. Inclusion of the multiple AGCMs is necessary to

enhance the confidence in the reliability of the results.

Based on their spatial structure and the corresponding principle component time-series, the three leading modes of SSTs included a trend mode, a Pacific and an Atlantic mode. Consistent with previous studies, and well documented global influence of SST variability in the tropical Pacific, the atmospheric influence of the Pacific modes was the largest. In the extratropics, and for the precipitation, the continental region of the US is one of the most sensitive regions to variations in the SST, and this conclusion was unanimous based on the analysis of the observed data, as well as AMIP and idealized AGCM simulations (Figs. 2-4). Our analysis also included changes in the PDF for the annual mean precipitation over the Great Plains region. The results indicate that the probability of precipitation deficit is largest for the cold phase of the Pacific SST mode, with the positive phase of the Atlantic SST mode also playing a role.

The reconstruction of the annual mean variability based on the response obtained from the idealized experiments had a close resemblance with response in the AMIP simulations where observed variations in the global SSTs are specified. This analysis attests to the fact that the SST modes identified herein, and their atmospheric influence, has a dominant contribution to the atmospheric response inferred in the AMIP simulations forced with observed global SSTs. This is further conformed based on the comparison of the time-series of the precipitation over the Great Plains (Fig. 7).

Based on the reconstruction approach, we also assess the role of differences in SST analysis, particularly their influence on the precipitation averaged over the Dust Bowl period. A

surprising conclusion from this analysis that for the SST reconstructed based on the HADISST were unable to capture the drying in the AMIP simulation. One possible explanation is that for the Dust Bowl period, the projection of HADISST on the modes of SST identified herein was small.

To the extent the precipitation variability could be associated with the occurrence of droughts, the results from the multi-model AGCM simulations have implications for drought variability and predictability, particularly over the US. Consistent with earlier studies (Hoerling and Kumar 2003; Schubert et al. 2004), the likelihood of droughts over the central US is greatly enhanced during the cold phase of Pacific SST mode, with potential for additional contribution from the positive phase from the Atlantic SST mode. Further, possible local feedbacks leading to warmer surface temperatures can further exacerbate the influence of precipitation deficit on the soil moisture and drought. Although the SST trend mode does not have an appreciable influence on the precipitation over the central US, the associated warmer surface temperature, and their influence on the surface evaporation, can also exacerbate the possibility of droughts.

The importance of the SST modes in controlling the precipitation and the drought variability also has relevance for ongoing efforts in initialized decadal predictions as part of the IPCC CMIP5 experimental design (Meehl et al. 2009). Since ultimately the prediction of SST modes discussed in this paper, is a coupled ocean-atmosphere problem, it will be imperative to monitor and assess predictability of the SST modes in the decadal prediction efforts. The analysis presented here lays the framework for understanding the remote influence of the modes of SST variability on the terrestrial climate, and documents the potential predictability associated with known structures of SST variability, to what extent the predictability can be

realized can next be examined based on the coordinated set of initialized decadal prediction runs.

Acknowledgment. This work was carried out as part of a U.S. CLIVAR drought working group activity supported by NASA, NOAA, and NSF to coordinate and compare climate model simulations forced with a common set of idealized SST patterns. The authors would like to thank NASA's Global Modeling and Assimilation Office (GMAO) for making the NSIPP1 runs available, the Lamont-Doherty Earth Observatory of Columbia University for making their CCM3 runs available, NOAA's Climate Prediction Center (CPC)/Climate Test Bed (CTB) for making the GFS runs available, NOAA's Geophysical Fluid Dynamics Laboratory (GFDL) for making the AM2.1 runs available, the National Center for Atmospheric Research (NCAR) for making the CAM3.5 runs available, and the Center for Ocean Land Atmosphere (COLA) and the University of Miami's Rosenstiel School of Marine and Atmospheric Science for making the CCSM3.0 coupled model runs available.

References

- Alexander, M.A., I. Bladé, M. Newman, J.R. Lanzante, N.C. Lau, and J.D. Scott, 2002: The Atmospheric Bridge: The Influence of ENSO teleconnections on air–sea interaction over the global oceans. *J. Climate*, **15**, 2205–2231.
- Bacmeister J., P. J. Pegion, S. D. Schubert, and M. J. Suarez, 2000: An atlas of seasonal means simulated by the NSIPP 1 atmospheric GCM. Vol. 17. NASA Tech. Memo. 104606, Goddard Space Flight Center, Greenbelt, MD, 194 pp.
- Brohan P., J. J. Kennedy, I. Harris, S. F. B. Tett, P. D. Jones, 2006: Uncertainty estimates in regional and global observed temperature changes: a new dataset from 1850. *J. Geophys. Res.* 111:D12106. doi:10.1029/2005JD006548
- Campana, K. and P. Caplan, Editors, 2005: Technical Procedure bulletin for T382 global forecast system (http://www.emc.ncep.noaa.gov/gc_wmb/Documentation/TPBoct05/T382.TPB.FINAL.htm).
- Chou, C., J. D. Neelin, J.-Y. Tu, C-T. Chen, 2006 : Regional tropical precipitation change mechanisms in ECHAM4/OPYC3 under global warming. *J. Climate*, **19**, 4207-4223.

Compo, G., and P. Sardeshmukh, 2008: Oceanic influences on recent continental warming, *Clim. Dyn.*, **32**, 333-342, doi:10.1007/s00382-008-0448-9.

Delworth et al., 2006: GFDL's CM2 global coupled climate models - Part 1: Formulation and simulation characteristics, *J. Climate*, **19**, 643-674.

Easterling, D. R., T. W. R. Wallis, J. H. Lawrimore, and R. H. Heim Jr., 2007: Effects of temperature and precipitation trends on U.S. drought. *Geophys. Res. Lett.* **34**, doi:10.1029/2007GL031541

Enfield, D.B., A.M. Mestas-Nuñez, and P.J Trimble, 2001: The Atlantic Multidecadal Oscillation and its relation to rainfall and river flows in the continental US. *Geophys. Res. Lett.*, **28**, 2077–2080.

The GFDL Global Atmospheric Model Development Team, 2004. The New GFDL Global Atmosphere and Land Model AM2-LM2: Evaluation with Prescribed SST Simulations. *J. Climate*, **17**, 4641-4673.

Hoerling, M. P., and A. Kumar, 2003: The perfect oceans for drought, *Science*, **299**, 691-694.

Hoerling, M. P., A. Kumar, J. Eischeid, and B. Jha, 2008: What is causing the variability in Global Land Temperature? *Geophys. Res. Lett.*, **35**, L23712, doi:10.1029/2008GL035984

- Kaiser, H. F. 1958: The Varimax Criterion for Analytic Rotation in Factor Analysis. *Psychometrika.*, **23**, 187-200.
- Kiehl, J.T., J.J. Hack, G. Bonan, B.A. Boville, D. Williamson and P. Rasch, 1998. The National Center for Atmospheric Research Community Climate Model: CCM3. *J. Climate*, **11**, 1131-1149.
- Kunkel, K. E., X.-Z. Liang, J. Zhu, and Y. Lin, 2006: Can CGCMs simulate the twentieth-century warming hole in the central United States? *J. Climate*, **19**, 4137-4153.
- Kumar, A., and M. P. Hoerling, 2000: Analysis of a conceptual model of seasonal climate variability and implications for seasonal predictions. *Bull. Amer. Meteor. Soc.*, **81**, 255-264.
- Kumar, A., F. Yang, L. Goddard, S. Schubert, 2004: Differing trends in the tropical surface temperatures and precipitation over land and oceans. *J. Climate*, **17**, 653-664.
- Mantua, N. J., S. R. Hare, Y. Zhang, J. M Wallace, and R. C. Francis R C, 1997: A Pacific interdecadal climate oscillation with impacts on salmon production. *Bull. Amer. Meteor. Soc.*, **78**, 1069-1079.
- Meehl, G. A., and Co-authors, 2009: Decadal Prediction: Can it be skillful. *Bull. Amer. Meteor. Soc.*, submitted.

- Milly, P. C. D., and A. B. Shmakin, 2002. Global modeling of land water and energy balances. Part I: The land dynamics (LaD) model. *J. Hydrometeorology*, **3**, 283-299.
- Namais, J., 1969: Seasonal Interactions Between the North Pacific and the Atmosphere During the 1960s. *Mon. Weather Rev.* **97**, 173-192.
- Namais, J., 1983: Some causes of the United States drought. *J. Clim. and Appl. Met.*, **22**, 30-39.
- Peng, P., A. Kumar, A. G. Barnston, and L. Goddard, 2000: Simulation skills of the SST-forced global climate variability of the NCEP-MRF9 and Scripps/MPI ECHAM3 models. *J. Climate*, **13**, 3657-3679.
- Power, S., T. Casey, C. Folland, A. Colman, and V. Mehta, 1999: Interdecadal modulation of the impact of ENSO on Australia. *Climate Dyn.*, **15**, 319–324.
- Rayner N. A., D. E. Parker, E. B. Horton, C. K. Folland, L. V. Alexander, D. P. Rowell, E. C. Kent, and A. Kaplan, 2003: Global analyses of sea surface temperature, sea ice and night marine air temperature since the late nineteenth century. *J. Geophys. Res.*, **108**, 4407, doi:10.1029/2002JD002670.
- Robinson, W. A., R. Reudy, and J. E. Hansen, 2002: On the recent cooling in the east-central United States. *J. Geophys. Res.*, **107**, 4748, doi:10.1029/2001JD001577.

- Saji, N. H., B. N. Goswami, P. N. Vinayachandran, and T. Yamagata 1999: A dipole mode in the tropical Indian Ocean, *Nature*, **401**, 360– 363.
- Schubert, S.D. M.J. Suarez, P.J. Pegion, R. D. Koster, and J.T. Bacmeister, 2004: Causes of long-term drought in the U.S. Great Plains., *J. Climate*, **17**, 485-503.
- Schubert, S. D., and Co-authors, 2009: A USCLIVAR project to assess and compare the responses of global climate models to drought-related SST forcing patterns: Overview and results. *J. Climate*, to appear.
- Seager, R., Y. Kushnir, C. Herweijer, N. Naik and J. Velez, 2005: Modeling tropical forcing of persistent droughts and pluvials: 1856-2000. *J. Climate*, **18**, 4068-4091.
- Smith, T., R. Reynolds, T. Peterson, J Lawrimore, 2008: Improvements to NOAA's Historical Merged Land-Ocean Surface Temperature Analysis (1880-2006), *J. Climate*, **21**, 2283-2296.
- Tang, Y., Z. Deng, X. Zhou, Y. Cheng, and D. Chen, 2008: Interdecadal variation of ENSO predictability in multiple models. *J. Climate*, **21**, 4811-4833.
- Wang, H. and Co-authors, 2009: Attribution of the seasonality and regionality in climate trends over the United States during 1950-2000, *J. Climate*, **22**, 2571-2590.
- Vose R., R. Schmoyer, P. Steurer, T. Peterson, R. Heim, T. Karl, and J. Eischeid, 1992: The

Global Historical Climatology Network: Long-term monthly temperature, precipitation, sea level pressure, and station pressure data. Carbon Dioxide Information Analysis Center, Oak Ridge National Laboratory ORNL/CDIAC-53, NDP-041, Oak Ridge, TN, 296 pp.

Xue, Y., T. Smith, R. Reynolds, 2003: Interdecadal changes of 30-yr SST normals during 1981-2000. *J. Climate*, **16**, 1601-1612.

Figures

Figure 1. The three leading rotated EOFs of HADISST annual mean SST for 1901-2004. Combined these three EOFs explain over 53% of the inter-annual variance. Contour interval for left panels is 0.1K with the zero contour omitted.

Figure 2. Composites of observed precipitation (left panels, from GHCN in mm/day) and surface air temperature (right panels, from HadCRUT3 in degrees K). Composites are based on +/- one standard deviation of the principal components in Fig. 1. White areas indicate areas of insufficient observations.

Figure 3. Same as figure 2, except for the multi-model ensemble mean of the AMIP runs.

Figure 4. The multi-model response to the three patterns, precipitation (left) and surface temperature (middle) and 200 mb height (left). Contours show the average of the response, and shading indicated where at least 4 out of the 5 models (3 out of 4 for the Trend patterns) produced the same sign response. Units are mm/day for precipitation, $^{\circ}$ K for temperature and meters for heights.

Figure 5. Probability density function of annual mean precipitation over the US Great Plains (95W-105W, 30N-50N) for all of the models combined (235 years of simulation for the Pacific forcing (top) and Atlantic forcing (middle), and 185 years for the trend pattern (bottom). Solid curve is from the warm (positive) forcing, and the dashed is for the negative pattern. The dotted line repeated in each panel is for the climatological SST simulations. Units are mm/day.

Figure 6. Temporal Correlation of annual mean precipitation between the multi-model AMIP mean and the reconstruction based on the idealized runs. Note how the precipitation over Central United states is the highest correlated mid-latitude region.

Figure 7. Time series of annual mean Great Plains precipitation, the multi-model Ensemble mean from the AMIP runs is the black dashed line, and the reconstruction based on the Model response to each of the 3 SST patterns is solid gray line. The precipitation value for each year is the sum of each pattern scaled by the principal components in figure 1.

Figure 8. Average SST anomaly from 1932-1938 from the original HADISST dataset (a) and from reconstruction of the first 3 REOFS (b). Lower panels are averages of the same period of the ERSSTv3b(c) and projection of the ERSST data onto the leading REOFS of the HADISST data (d). Contour interval is 0.1 K with the zero contour omitted.

Figure 9. Precipitation (left) and surface temperature (right) anomalies averaged for the period of 1932-1938. Top row is from the AMIP MMM. Middle row is from projecting the ERSSTv3b SST data onto the 20 leading REOFS of HADISST, and reconstructing the temperature and precipitation anomalies from the linear response to these patterns. 3rd row is same as the 2nd, expect for projection of the HADISST data. 4th row is the observed composites.

Tables

Table 1. Model data availability for the long AMIP simulations.

Table 2. Probability of having 3-years in a row with below average precipitation by sampling any 3-years at random for each experiment.

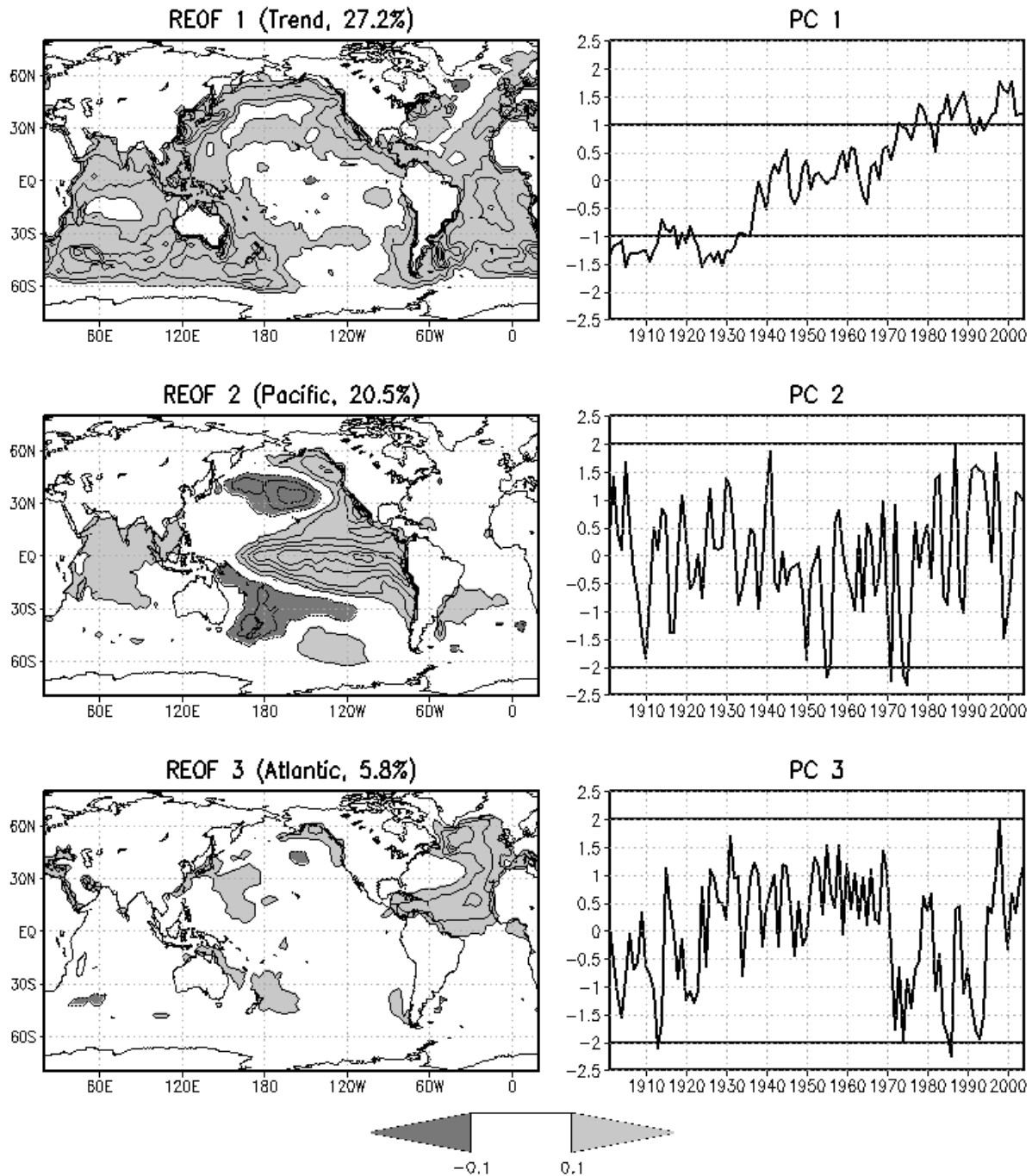


Figure 1. The three leading rotated EOFs of HADISST annual mean SST for 1901-2004. Combined these three EOFs explain over 53% of the inter-annual variance. Contour interval for left panels is 0.1K with the zero contour omitted.

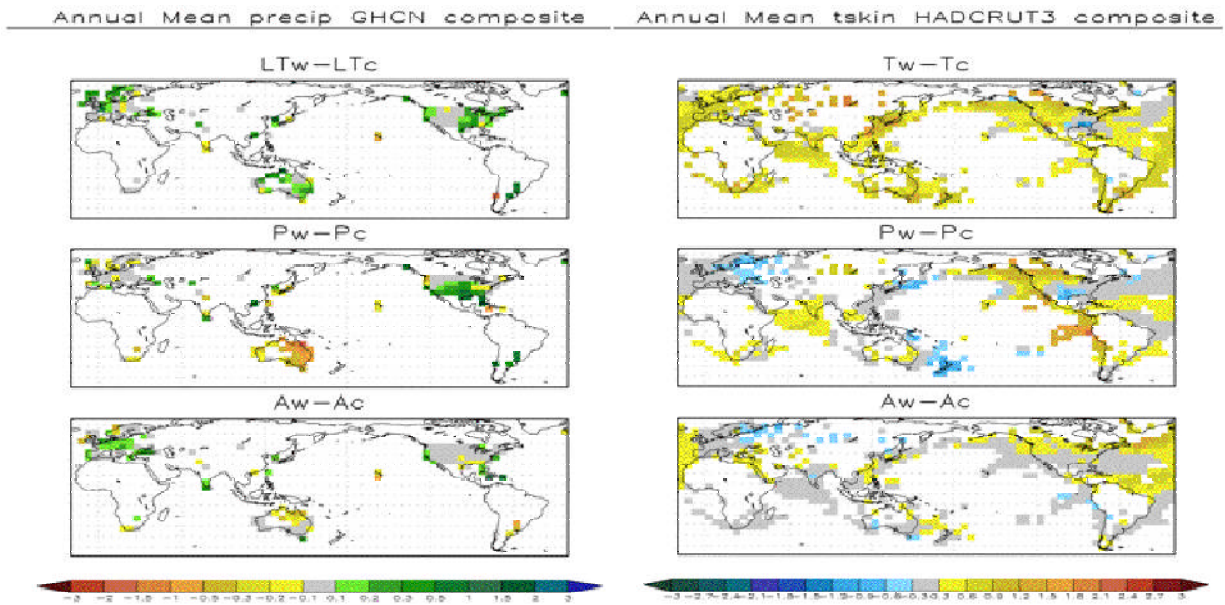


Figure 2. Composites of observed precipitation (left panels, from GHCN in mm/day) and surface air temperature (right panels, from HadCRUT3 in degrees K). Composites are based on +/- one standard deviation of the principal components in Fig. 1. White areas indicate areas of insufficient observations.

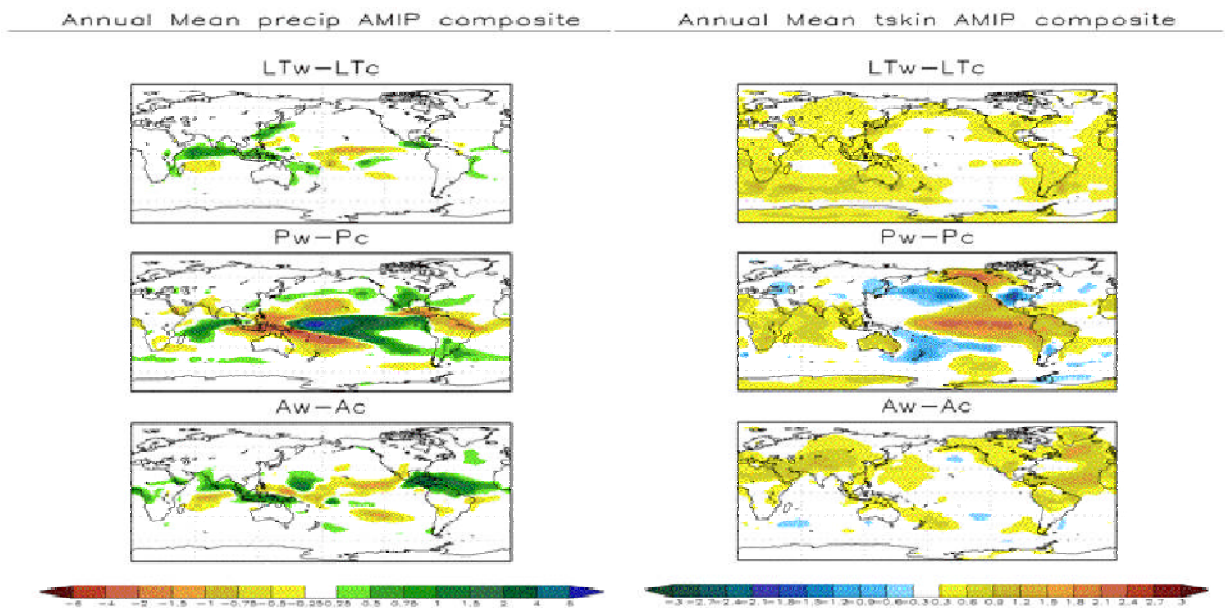


Figure 3. Same as figure 2, except for the multi-model ensemble mean of the AMIP runs.

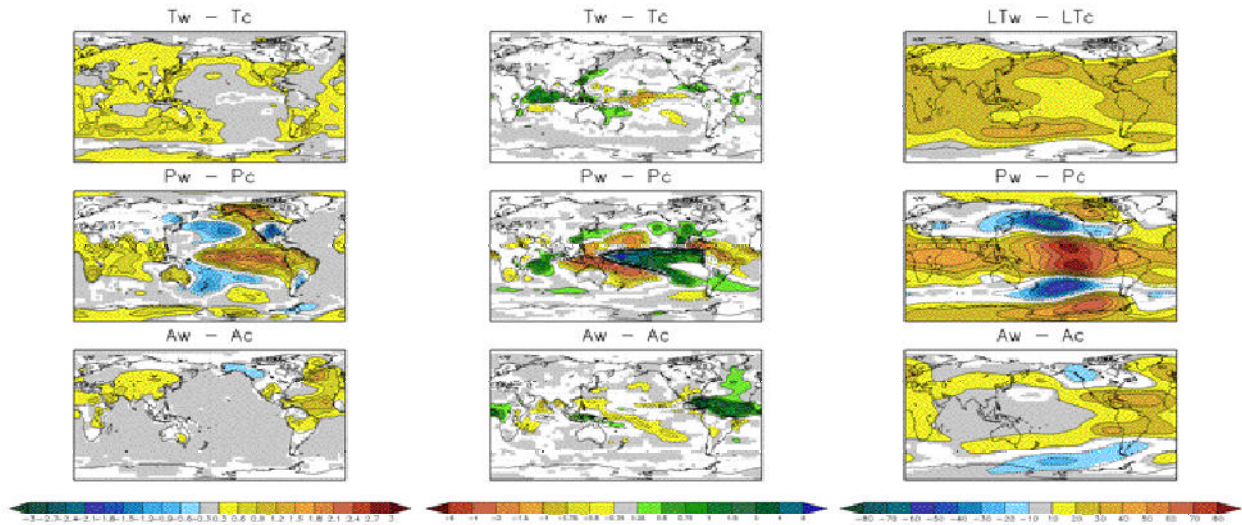


Figure 4. The multi-model response to the three patterns, precipitation (left) and surface temperature (middle) and 200 mb height (left). Contours show the average of the response, and shading indicated where at least 4 out of the 5 models (3 out of 4 for the Trend patterns) produced the same sign response. Units are mm/day for precipitation, $^{\circ}\text{K}$ for temperature and meters for heights.

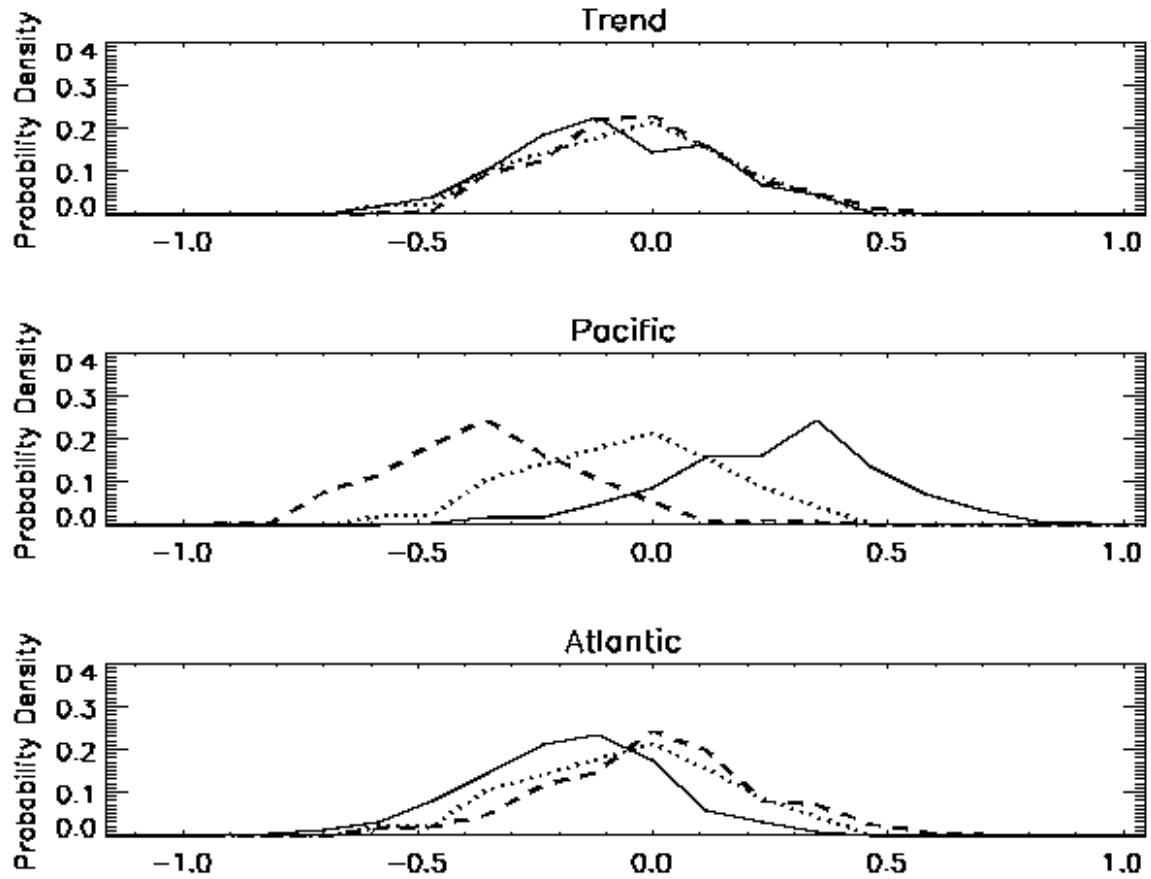


Figure 5. Probability density function of annual mean precipitation over the US Great Plains (95W-105W, 30N-50N) for all of the models combined (235 years of simulation for the Pacific forcing (top) and Atlantic forcing (middle), and 185 years for the trend pattern (bottom). Solid curve is from the warm (positive) forcing, and the dashed is for the negative pattern. The dotted line repeated in each panel is for the climatological SST simulations. Units are mm/day.

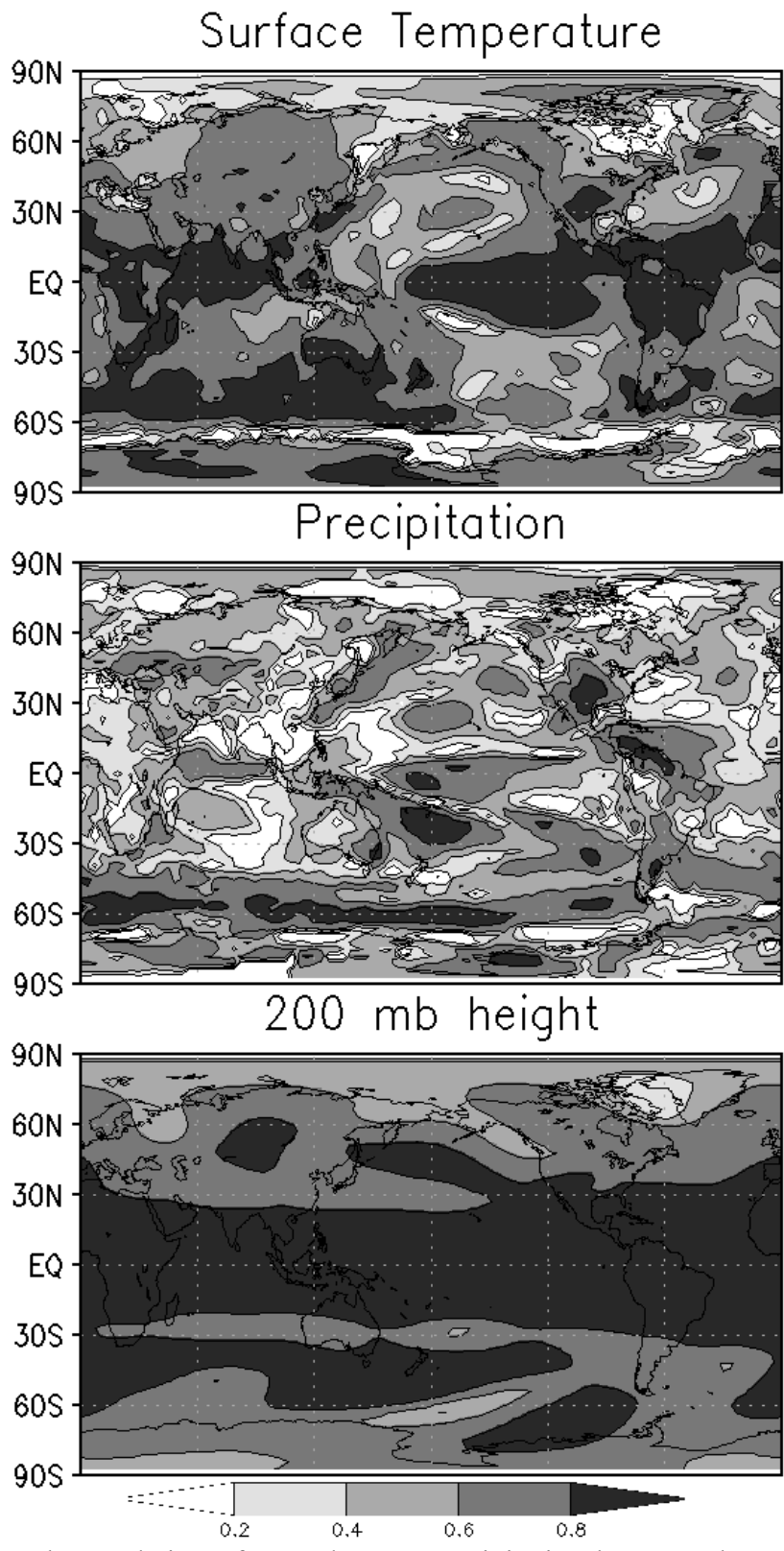


Figure 6. Temporal Correlation of annual mean precipitation between the multi-model AMIP mean and the reconstruction based on the idealized runs. Note how the precipitation over Central United states is the highest correlated mid-latitude region.

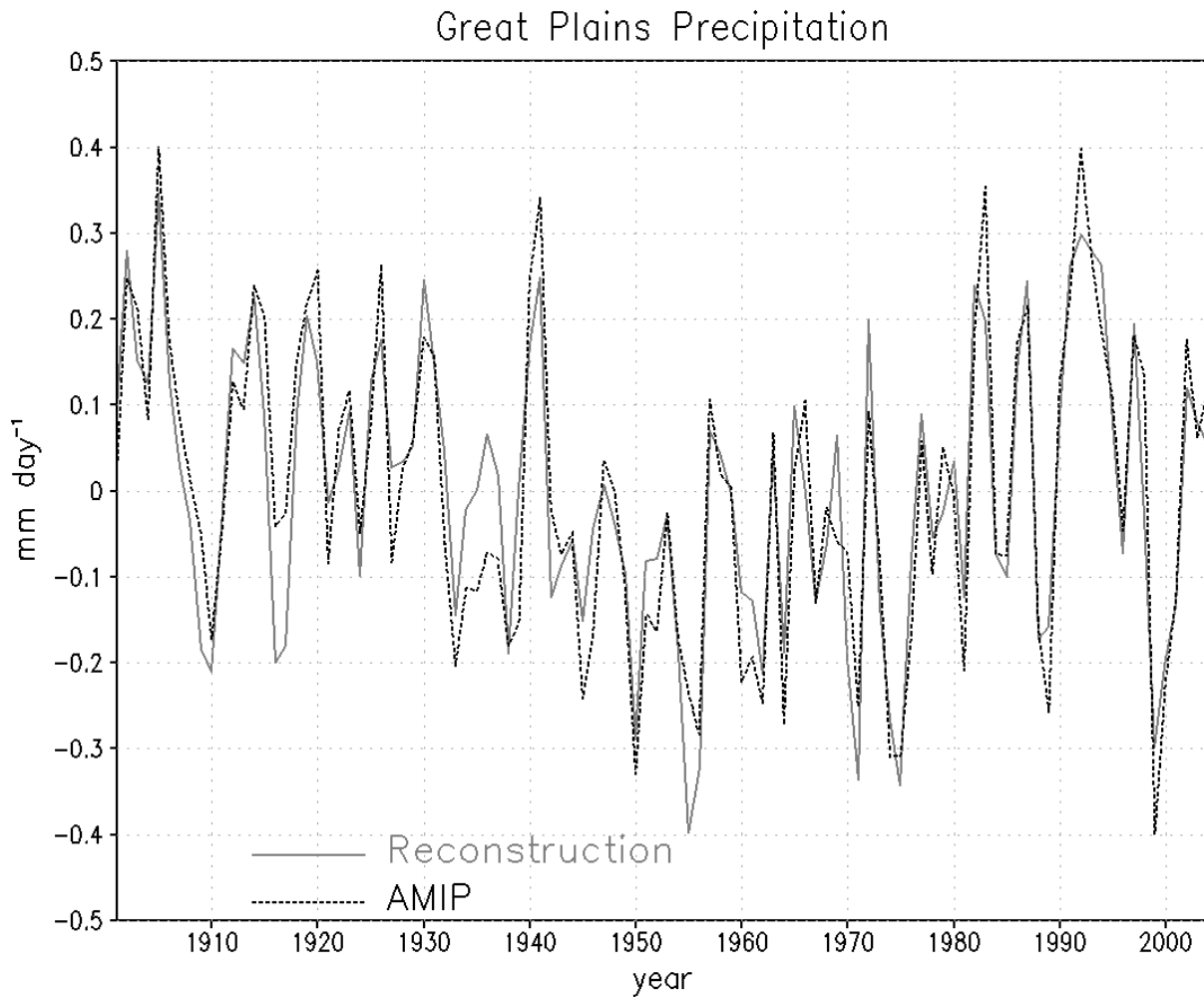


Figure 7. Time series of annual mean Great Plains precipitation, the multi-model Ensemble mean from the AMIP runs is the black dashed line, and the reconstruction based on the Model response to each of the 3 SST patterns is solid gray line. The precipitation value for each year is the sum of each pattern scaled by the principal components in figure 1.

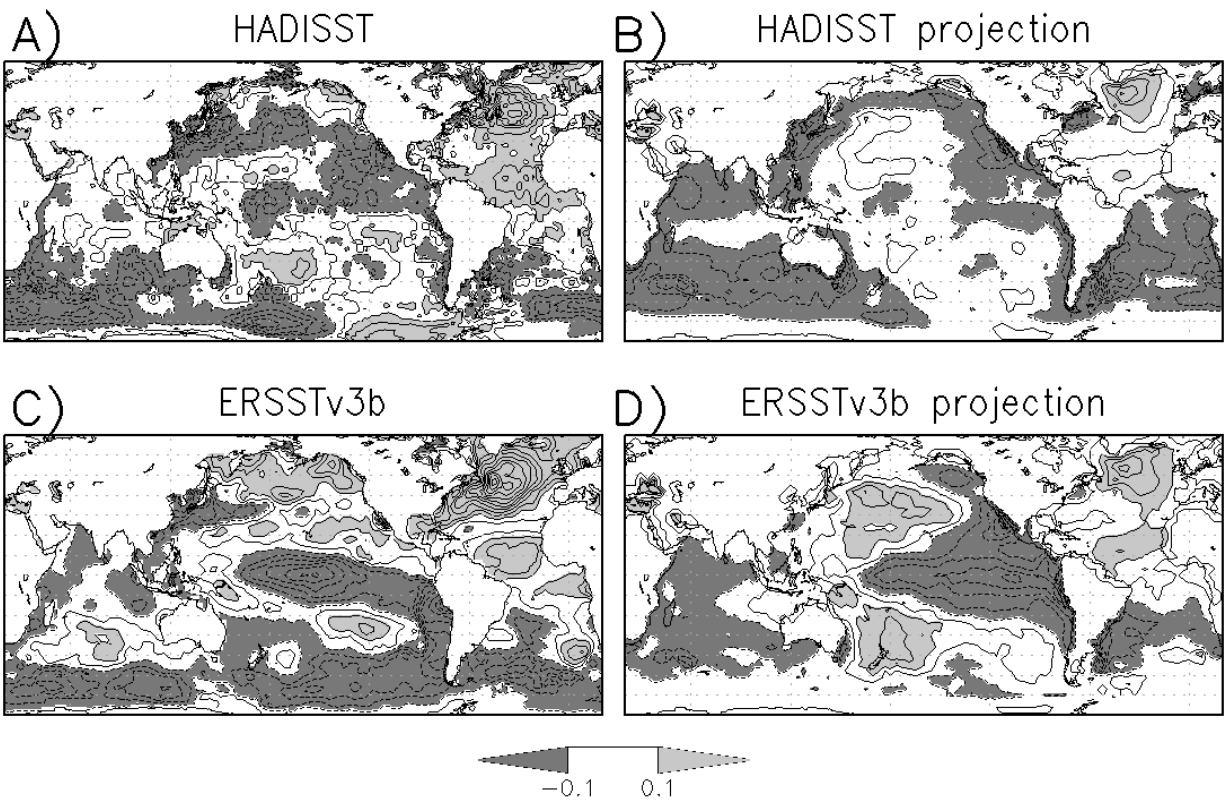


Figure 8. Average SST anomaly from 1932-1938 from the original HADISST dataset (a) and from reconstruction of the first 3 REOFS (b). Lower panels are averages of the same period of the ERSSTv3b(c) and projection of the ERSST data onto the leading REOFS of the HADISST data (d). Contour interval is 0.1 K with the zero contour omitted.

1932–1398 Composite

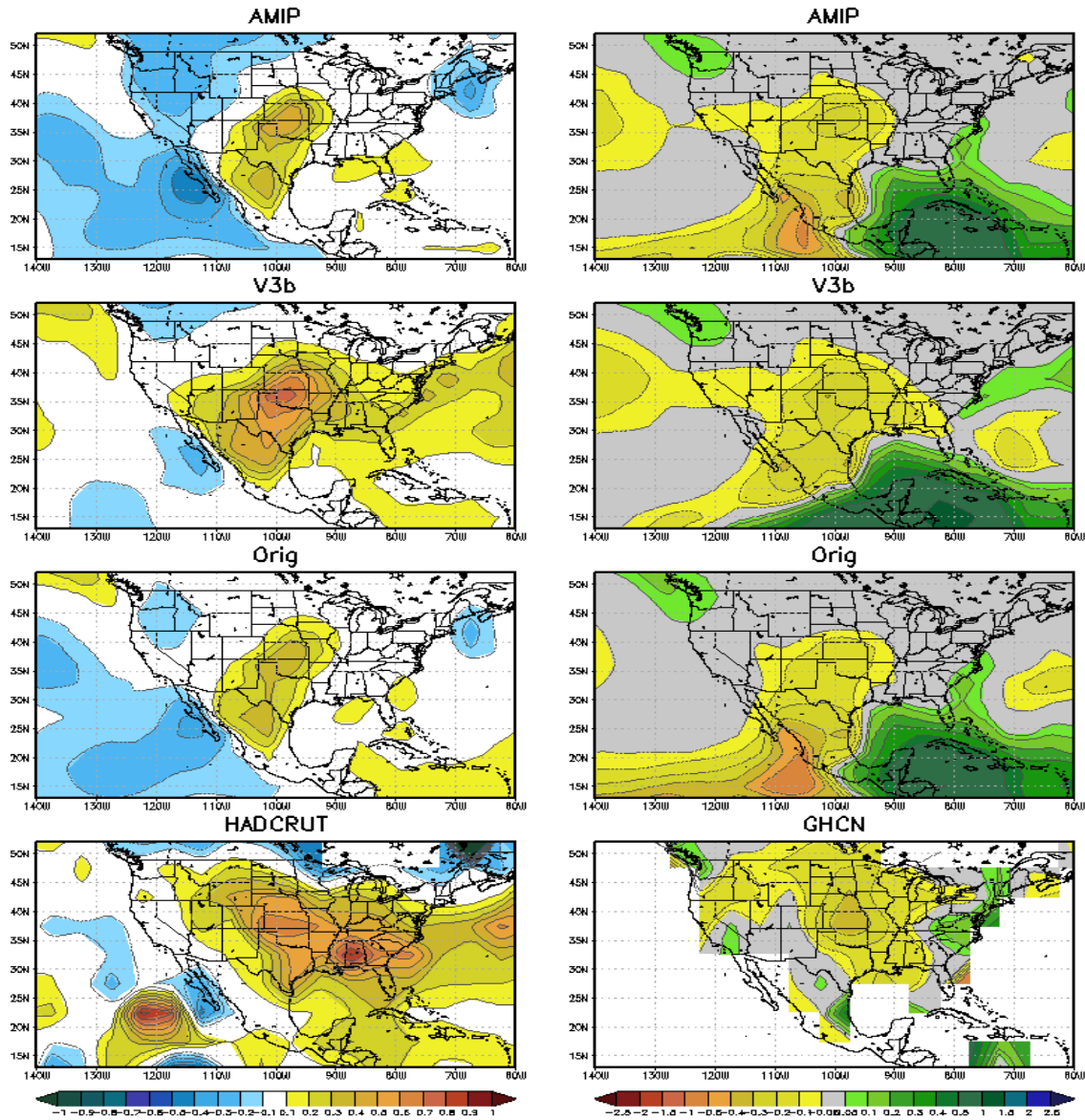


Figure 9. Precipitation (left) and surface temperature (right) anomalies averaged for the period of 1932-1938. Top row is from the AMIP MMM. Middle row is from projecting the ERSSTv3b SST data onto the 20 leading REOFS of HADISST, and reconstructing the temperature and precipitation anomalies from the linear response to these patterns. 3rd row is same as the 2nd, expect for projection of the HADISST data. 4th row is the observed composites.

Model	Number of Ensemble Members	Simulated years
NASA/NSIPP	14	1902-2004
LDEO/CCM3	16	1856-2006
GFDL/AM2.1	10	1870-1999
NCAR/CCM3.5	1	1901-2004

Table 1. Model data availability for the long AMIP simulations.

	NW	SW	NE	SE	GP
Tw	9.3	23.4	9.7	19.4	24.0
Tc	15.8	13.1	17.7	10.0	6.7
Pw	6.6	0.4	3.7	3.2	0.1
Pc	17.7	51.2	24.5	53.6	78.9
Aw	9.4	38.8	16.1	37.9	36.5
Ac	19.0	7.4	8.	12.0	3.5
Clim	15.7	17.7	12.1	9.5	13.0

Table 2. Probability of having 3-years in a row with below average precipitation by sampling any 3-years at random for each experiment.